RWS

Phys. Med. Biol. 41 (1996) 111–124. Printed in the UK

stoichiometric calibration CT → stopping power

The calibration of CT Hounsfield units for radiotherapy treatment planning

Uwe Schneider†§, Eros Pedroni‡ and Antony Lomax‡

† Medical Physics Group, Section of Physics, University of Munich, Garching, Bavaria, Germany
‡ Department of Radiation Medicine, Paul Scherrer Institute, Villigen, Switzerland

Received 23 February 1995

Abstract. Computer tomographic (CT) scans are used to correct for tissue inhomogeneities in radiotherapy treatment planning. In order to guarantee a precise treatment, it is important to obtain the relationship between CT Hounsfield units and electron densities (or proton stopping powers for proton radiotherapy), which is the basic input for radiotherapy planning systems which consider tissue heterogeneities. A method is described to determine improved CT calibrations for biological tissue (a stoichiometric calibration) based on measurements using tissue equivalent materials. The precision of this stoichiometric calibration and the more usual tissue substitute calibration is determined by a comparison of calculated proton radiographic images based on these calibrations and measured radiographs of a biological sample. It has been found that the stoichiometric calibration is more precise than the tissue substitute calibration.

1. Introduction

Calibrated computer tomographic (CT) data are the basic input for radiotherapy treatment planning systems which take into account the effect of tissue inhomogeneities. The accuracy of dose calibrations based on such CT data is partly determined by the precision of the calibration of CT Hounsfield units to relative electron density (Constantinou and Harrington 1992) or to relative proton stopping power for proton radiotherapy. The error of the final electron density distribution originates from a number of sources. Firstly the measurement of the Hounsfield value of homogeneous material can vary between 1 and 2% (Constantinou and Harrington 1992) and is also dependent on the location of the material in the image, a variation that can reach up to 3% (Moyers *et al* 1993). In addition, the measurement of high CT numbers can vary from scanner to scanner and can strongly influence the calibration. Constantinou and Harrington (1992) found a 10% deviation in electron density dependent on the type of scanner. It is also known that scanner specific parameters such as the photon energy, the scan diameter and the matrix size may affect the measurement of the CT number. However, McCullough and Holmes (1985) found no significant change in the Hounsfield numbers while changing these. A final source of error is the approximation of real tissue with tissue substitutes used for the measurement of the relationship of Hounsfield units to electron densities. The chemical composition of commonly used tissue substitutes is different to that of real tissue. To create usable samples the oxygen, carbon, hydrogen and calcium content are changed resulting in significantly different values for electron density,

§ Current address: Department of Radiation Oncology and Nuclear Medicine, City Hospital Triemli, 8063 Zurich, Switzerland.

0031-9155/96/010111+14$19.50

proton stopping power and Hounsfield values. Tissue substitutes are usually produced for their use in radiation dosimetry and radiobiology and not for calibrating CT images.

A possible solution of this problem is a stoichiometric calibration which is presented in this paper. In such a stoichiometric method both the measured Hounsfield units of tissue substitutes and the chemical composition of real tissues are used to predict Hounsfield values for human tissues.

Additionally, we report on the verification of the stoichiometric calibration using range calibrated proton radiographic measurements of a biological sample (a sheep's head). The CT numbers of the sheep's head were measured and converted to relative proton stopping power by using both a tissue substitute calibration and the stoichiometric calibration. The comparison of measurements and calculations of the integrated proton stopping power showed that the stoichiometric calibration is more precise than tissue substitute calibrations for proton radiotherapy.

It is also shown that the relative proton stopping power for biological tissues and tissue substitutes is equivalent to the relative electron density within a few per cent. Hence stoichiometric calibrations could be an improvement for x-ray radiotherapy and should be applied to x-ray radiotherapy treatment planning also.

2. Calibration of CT numbers

2.1. Tissue substitute calibration

2.1.1. X-ray radiotherapy. In this section, the calibration from CT Hounsfield units to relative electron densities, using tissue equivalent samples, will be described. To obtain this relationship we have calculated the relative electron densities of various tissue substitutes (ICRU 1989, Constantinou 1974) taking into account their chemical composition (tables 1 and 3) using

$$\rho_e = \rho N_g / \rho^{water} N_g^{water} \tag{1}$$

where ρ is the density and N_g is the number of electrons per unit volume of the mixture given by

$$N_g = \sum N_g^i = N_A \sum \frac{\omega_i Z_i}{A_i} \tag{2}$$

where N_A is Avagadro's number Z_i and A_i are the atomic number and atomic weight of the ith element and ω_i is its proportion by weight. The tissue substitutes of table 1 have also been scanned in a GE 9000 scanner at 120 kVp to obtain the corresponding Hounsfield values.

The usual form of the calibration is a bilinear relationship between relative electron density and CT units. For Hounsfield numbers up to water ($H = 1000$; sometimes also up to $H = 1050$) a mixture of water and air is assumed. Scaled Hounsfield values greater than 1000 or 1050 are assumed to be a mixture of bone substitutes and water (McCullough and Holmes 1985, Battista *et al* 1980).

2.1.2. Proton therapy. The determination of the tissue substitute calibration curve for proton treatment planning follows the same procedure as for x-rays (Chen *et al* 1979, Mustafa and Jackson 1983). As for proton dose calculations the required information is the relative proton stopping power this is calculated using the Bethe–Bloch formula (Bichsel 1972), which can be approximated by

$$\rho_s = \rho_e \{\log[2m_e c^2 \beta^2 / I_m (1-\beta^2)] - \beta^2\} / \{\log[2m_e c^2 \beta^2 / I_{water}(1-\beta^2)] - \beta^2\} = \rho_e K \tag{3}$$

Table 1. Chemical compositions (percentage weights) of various tissue substitutes used for the measurements.

		H	C	N	O	F	Na	Mg	P	S	Cl	K	Ca
Atomic number		1	6	7	8	9	11	12	15	16	17	19	20
Atomic weight		1.0079	12.011	14.006	15.999	18.998	22.989	24.312	30.973	32.064	35.450	39.102	40.080
Material	Substitute for	Composition in % of weight											
AP 6	Fat	8.36	69.14	2.36	16.94	3.07					0.14		
Water		11.19			88.81								
MS/SR 4	Muscle	9.5	70.25	3.48	15.15		0.08	0.02	0.18	0.50	0.12	0.30	0.01
IB/SR 1	Inner bone	8.73	63.19	2.36	17.83		0.06		2.62		0.12		5.09
TSK/SR 1	Skeleton	6.4	46.4	2.80	26.4		0.30	0.10	7.0	0.20	0.10	0.20	10.0
HB/SR 4	Hard bone	4.45	29.09	3.88	31.93		0.06	0.21	10.0	0.32	0.06		19.99

where βc is the velocity of the proton, m_e is the mass of the electron and I_m is the mean ionization energy of the target atoms. The ionization energy I_i for each element was taken from the tables of Janni (1982) and the mean ionization energy for a mixture was calculated using the Bragg additivity rule as follows:

$$\ln I_m = \left(\sum \frac{\omega_i Z_i}{A_i} \ln I_i\right)\left(\sum \frac{\omega_i Z_i}{A_i}\right)^{-1}. \tag{4}$$

Additionally the relative proton stopping powers of the tissue substitutes listed in table 1 have been measured using a 219 MeV proton beam. Measured and calculated ρ_s values coincide within 1.6% and are listed in table 2. The conversion curve for proton treatment planning is usually obtained following the procedure described in the previous section.

Table 2. Measured and calculated Hounsfield numbers H, densities ρ, relative electron densities ρ_e and relative proton stopping powers ρ_s for different materials used for measurements. K is ρ_s/ρ_e. ρ_s is also calculated for a 10% variation of the ionization potential; the numbers in brackets are the percentage deviations of ρ_s for such a variation.

Material	ρ (g cm^{-3})	H measured	H theory	ρ_e	ρ_s measured	ρ_s with $1.0I_m$	ρ_s with $0.9I_m$	ρ_s with $1.1I_m$	K
AP 6	0.91	856	865	0.885	0.89	0.907	0.918 (1.2%)	0.897 (1.1%)	1.025
Water	1.00	1000	1000	1.000	—	1.000			1.000
MS/SR 4	1.07	1027	1029	1.049	1.08	1.079	1.093 (1.2%)	1.067 (1.1%)	1.029
IB/SR 1	1.15	1214	1179	1.123	1.15	1.145	1.159 (1.2%)	1.132 (1.1%)	1.019
TSK/SR 1	1.32	1466	1440	1.259	1.28	1.257	1.272 (1.3%)	1.242 (1.1%)	0.998
HB/SR 4	1.48	1783	1791	1.386	—	1.352	1.369 (1.3%)	1.336 (1.2%)	0.975

2.1.3. Comparison of x-ray and proton calibration. It is of interest to compare the relative proton stopping powers with the relative electron densities for different types of tissue.

The relation between ρ_e and ρ_s is defined by the factor K in equation (3). We list in the last column of table 2 the values of K computed according to equation (3) for the different tissue substitutes and 219 MeV protons.

The error of the ρ_s calculation is governed by the uncertainty of the ionization potential. Hence, in table 2 we show for the six materials that K is rather insensitive to the value of the ionization potential I. A variation of the ionization potential by 10% changes the relative proton stopping power by less than 1.5%, which implies that the computation of K in formula (3) is precise. The fact that K is close to one suggests that proton stopping power and electron density relative to water track one another very closely.

2.2. Stoichiometric calibration

To improve the precision of the transformation of CT numbers, the tissue substitute calibration described in subsections 2.1.1 and 2.1.2 of the CT data was changed. From the known chemical composition of the tissue substitutes and the measurements of their Hounsfield values the response of the CT unit was parametrized by fitting the dependence of the photon attenuation as a function of the atomic number of the elemental composition of these materials. In this section we describe this process in detail.

A CT image represents the spatial distribution of photon attenuation coefficients. The scaled Hounsfield number is defined by

$$H = 1000\ \mu/\mu_w \tag{5}$$

where μ is the linear attenuation coefficient of the material and μ_w the coefficient for water.

wo effects which can be the attenuation of a photon beam for energies up to ~ These are (
toelectric absorption and scattering. The cross-section of scattering processes 1 MeV, pho
tled into that due to incoherent scattering and coherent scattering. The total can be divi
coefficient can be written in the form (Jackson and Hawkes 1981) attenuation

$$\mu = \rho N_g(Z, A)\{\sigma^{ph} + \sigma^{coh} + \sigma^{incoh}\} \quad (6)$$

is the electron density and σ^{ph}, σ^{coh} and σ^{incoh} the cross-sections for where ρN_g
c effect, coherent scattering and incoherent scattering respectively. An accurate photoelectri
tion of these cross-sections is given by Rutherford *et al* (1976) parametriza

$$\mu = \rho N_g(Z, A)\{K^{ph}Z^{3.62} + K^{coh}Z^{1.86} + K^{KN}\} \quad (7)$$

and K^{coh} are constants which characterize the different cross-sections and where K^{ph}
Klein–Nishina cross section. The energy dependent factors are included in K^{KN} is the
nts K^{ph}, K^{coh} and K^{KN} as opposed to the formulation of Rutherford *et al*. For the coefficie
f elements the attenuation coefficient can be obtained by the following formula a mixture o
d Hawkes 1981): (Jackson an

$$\mu = \rho N_g(Z, A)\{K^{ph}\tilde{Z}^{3.62} + K^{coh}\hat{Z}^{1.86} + K^{KN}\} \quad (8)$$

where

$$\tilde{Z} = \left[\sum \lambda_i Z_i^{3.62}\right]^{1/3.62} \quad (9)$$

$$\hat{Z} = \left[\sum \lambda_i Z_i^{1.86}\right]^{1/1.86} \quad (10)$$

and

$$\lambda_i = N_g^i/N_g. \quad (11)$$

measurements of H for different tissue substitutes of known chemical By making
(table 1) with a fixed energy of 120 kVp, we can determine from a linear composition
it of the experimental data to formulae (5) and (8) the constants K^{ph}, K^{coh} regression f
figure 1). These have been determined to be 1.227×10^{-5}, 4.285×10^{-4} and and K^{KN} (
vely. In figure 1 we show the measured Hounsfield values as a function of the 0.5 respecti
umbers. calculated n

e investigated a large variety of both tissue substitutes (table 3) and human We hav
le 4) as listed in *ICRU Report 44* and *ICRP Report 23*, respectively, and have tissues (tabl
with our parametrization of the CT unit (formulae (5) and (8)) values of H calculated
aterials. In addition we have calculated the relative electron densities of these for these m
sing equation (1) and the relative proton stopping powers at 219 MeV using materials us
). These too, are listed in tables 3 and 4. The data points are plotted in figures 2 equation (3
and 3.

ichiometric calibration can now be obtained by plotting for the human tissues The sto
le 4 the relative proton stopping power or the relative electron density against listed in tab
eld values. An appropriate curve may be fitted to these points. We decided the Hounsfi
three linear fits to obtain the calibration as shown in figure 2 as the solid to combine
irst linear curve fits the lung data ($0 < H < 850$), the second various organs line. The fi
< 1060) and the last bone tissue ($H > 1060$). As the data point of adipose ($1023 < H$
not lie on a curve connecting linearly the lung fit and the organ fit we decided tissue does
he lung fit with the fat data point ($850 < H < 930$) and the fat data point with to connect t
t ($930 < H < 1023$) to account for adipose tissue too. the organ fi

Table 3. Chemical composition as percentages, density ρ (taken from ICRU 1989) and calculated Hounsfield numbers, relative electron densities ρ_e and relative proton stopping powers ρ_s for various tissue substitutes.

	H	C	N	O	Ca	P	Na	Mg	S	Cl	K	F	Sb	Sn	ρ	H	ρ_e	ρ_s
A150	10.1	77.7	3.5	5.2	1.8							1.7			1.12	1098	1.108	1.145
Acrylic	8.0	60.0		32.0											1.17	1114	1.136	1.158
Alderson–lung	5.7	74.0	2.0	18.1									0.2		0.32	314	0.304	0.310
Alderson–muscle A	8.9	66.8	3.1	21.1									0.1		1.00	982	0.979	1.004
Alderson–muscle B	8.8	64.4	4.1	20.4						2.2			0.1		1.00	995	0.977	1.023
AP6	8.4	69.1	2.4	16.9						0.1		3.1			0.91	875	0.885	0.907
AP/L2	12.1	29.3	0.8	57.4	0.002	0.2	0.1	0.002		0.1	0.03				0.92	917	0.927	0.943
AP/SF1	12.0	75.5	0.8	11.1	0.02	0.01	0.1		0.1	0.4	0.03				0.92	901	0.926	0.962
B100	6.6	53.7	2.2	3.2	17.7							16.7			1.45	1665	1.380	1.380
B110	3.7	37.1	3.2	4.8	26.3							24.9			1.79	2203	1.649	1.609
BR12	8.7	69.9	2.4	17.9	1.0					0.1					0.97	936	0.948	0.973
Ethoxyethanol	11.2	53.3		35.5											0.93	910	0.930	0.954
EVA-28	12.3	77.3		10.4											0.95	929	0.959	0.998
Frigerio gel	10.0	12.0	4.0	73.3			0.4		0.2	0.1					1.12	1106	1.108	1.110
Frigerio liquid	10.2	12.3	3.5	72.9	0.01	0.2	0.1	0.02	0.3	0.1	0.4				1.08	1073	1.070	1.073
Glycerol trioleate	11.8	77.3		10.9											0.92	896	0.924	0.960
Goodman liquid	10.2	12.0	3.6	74.2											1.07	1056	1.061	1.064
Griffith breast	9.4	61.9	3.6	24.5	0.6			0.01						0.01	1.10	1068	1.082	1.109
Griffith lung	8.0	60.8	4.2	24.8	2.1			0.1						0.02	0.26	255	0.253	0.257
Griffith muscle	9.0	60.2	2.8	26.6	1.4									0.01	1.12	1095	1.098	1.122
M3	11.4	65.6		9.2	0.3			13.5							1.05	1050	1.050	1.079
Magnesium								100							1.74	1859	1.547	1.434
Mylar/Melinex	4.2	62.5		33.3											1.40	1291	1.313	1.322
Nylon-6	9.8	63.7	12.4	14.1											1.13	1086	1.115	1.147
Paraffin wax	15.0	85.0													0.93	925	0.961	1.011
Plaster of Paris	2.3			55.8	23.3				18.6						2.32	3022	2.135	2.017
Polyethylene	14.4	85.6													0.92	911	0.946	0.993
Polysterene	7.7	92.3													1.05	983	1.017	1.051
PTFE		24.0										76.0			2.10	1869	1.816	1.753
PVC	4.8	38.5								56.7					1.35	1717	1.245	1.207

Table 3. (Continued)

	H	C	N	O	Ca	P	Na	Mg	S	Cl	K	F	Sb	Sn	ρ	H	ρ_e	ρ_s
RF-1	14.1	84.1		0.9	0.6			0.3							0.93	926	0.953	1.000
Rice powder	6.2	44.4		49.4											0.84	797	0.806	0.810
RM-1	12.2	73.4		6.4	2.0			6.0							1.03	1041	1.038	1.075
RM/G1	10.2	9.4	2.4	77.4		0.03	0.1		0.1	0.2	0.2				1.07	1062	1.061	1.062
RM/L3	10.2	12.8	2.2	74.1		0.03	0.1		0.2	0.2	0.2				1.04	1031	1.031	1.034
RM/SR4	10.1	73.6	2.2	13.7		0.03	0.01	0.003	0.1	0.1	0.2				1.03	994	1.020	1.053
Rossi gel	9.8	15.7	3.6	70.9											1.10	1081	1.086	1.090
Rossi liquid	9.8	15.6	3.6	71.0											1.11	1090	1.096	1.100
RW-1	13.2	79.4		3.8	2.7			0.9							0.97	986	0.987	1.028
SB5	2.6	30.6	1.0	38.9	26.8					0.1					1.87	2313	1.726	1.674
Witt liquid	4.7			56.8		10.9					27.6				1.72	2144	1.604	1.535
WT1	8.1	67.2	2.4	19.9	2.3					0.1					1.02	996	0.991	1.013

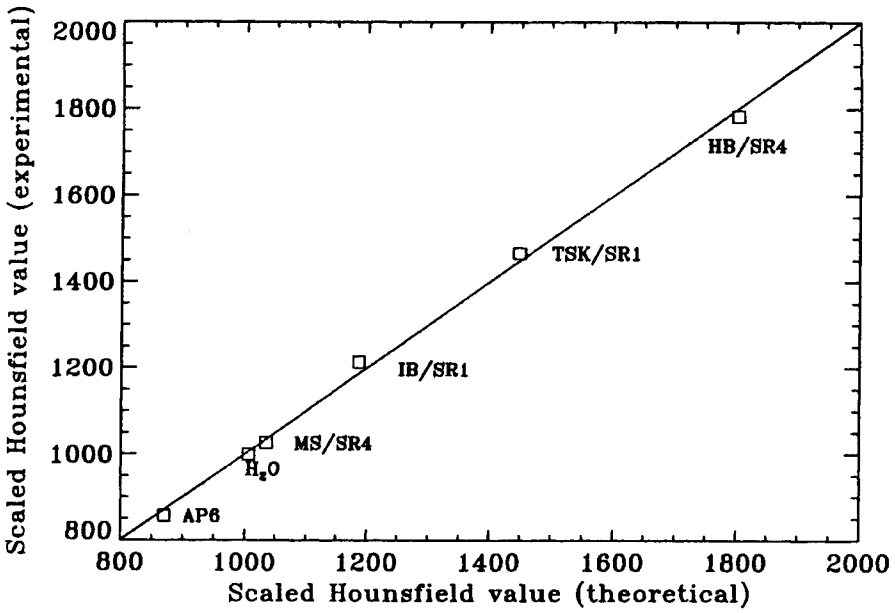

Figure 1. Experimental Hounsfield values versus calculated Hounsfield values obtained from a fit to formulae (5) and (8).

3. Measurements of integrated relative proton stopping power through a sheep's head

We have measured relative proton stopping power in a biological sample. This is of direct interest in checking the calibration of Hounsfield units to relative proton stopping power and, because K is close to one (subsection 2.1.3), it is also of interest for the calibration to relative electron densities for x-ray radiotherapy treatment planning.

The integrated relative stopping power ρ_s of 219 MeV protons penetrating through a sheep's head was measured by a method described in detail elsewhere (Schneider and Pedroni 1994). In brief, the sheep's head was cut from the body and fastened in moulage material with water equivalent properties. The transmitted range of protons penetrating through a sheep's head were obtained everywhere within the cross-sectional area of the beam. When these ranges are divided by the geometrical thickness of the sample, the average relative proton stopping power of the material along the proton trajectory can be determined. The result of such a proton radiographic measurement is a two-dimensional matrix of the integrated relative stopping powers of the sheep's head.

The sheep's head was scanned in addition in the same CT scanner which was used for the tissue substitute measurements described in subsection 2.1.2. The resulting CT data were converted into relative proton stopping power using the different techniques described previously. The CT numbers of the moulage material were converted to relative proton stopping power by measuring in an additional experiment its ρ_s value. The proton radiography was then simulated by integrating through the three-dimensional CT volume in the direction of the proton beam to obtain a two-dimensional projection of proton stopping powers. The simulated proton radiography was then compared with the measured radiography. An inaccurate calibration of the CT data is expected to show up as a deviation

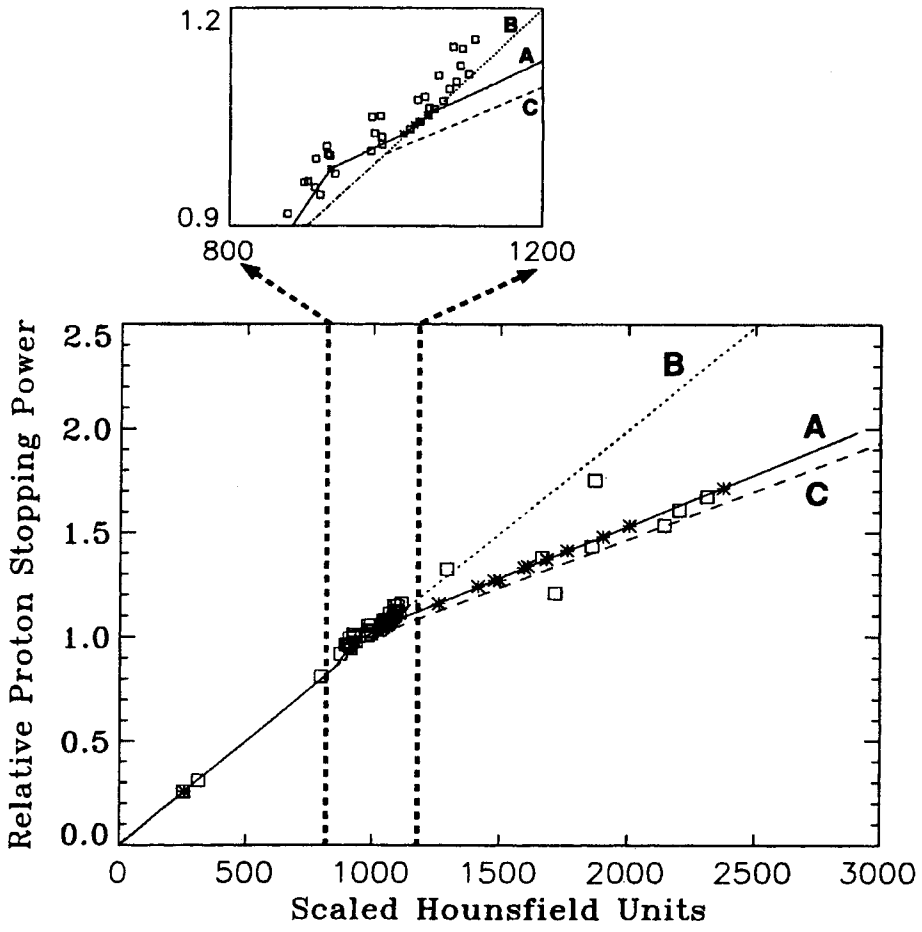

Figure 2. Calibration curves for the transformation of Hounsfield values into relative proton stopping power (ρ_s). The solid line shows the stoichiometric calibration (A) for biological tissues, the dotted line the tissue substitute calibration for Mylar/Melinex/PTFE (B) and the dashed line the tissue substitute calibration for B110/SB5 (C). The squares represent calculations for tissue substitutes and the stars are calculations based on the chemical composition of real tissues. The small plot shows in detail the Hounsfield number range corresponding to soft tissue.

between the simulated proton radiography and the experimentally obtained integral proton stopping power matrix.

4. Results

4.1. Comparison of tissue substitutes with real tissues

In figure 2 the relative proton stopping power of tissue substitutes (squares) listed in table 3 and real tissues (stars) listed in table 4 are plotted against the scaled Hounsfield values. It can easily be seen that the tissue substitute data vary substantially. Hence, a

Table 4. Chemical composition as percentages, density ρ (taken from ICRP 1975) and calculated Hounsfield numbers, relative electron densities ρ_e and relative proton stopping powers ρ_s for various tissue descriptions.

	H	C	N	O	Ca	P	Na	Mg	S	Cl	K	Fe	I	ρ	H	ρ_e	ρ_s
Adipose tissue	11.4	59.8	0.7	27.8			0.1		0.1	0.1				0.95	930	0.951	0.979
Blood	10.2	11.0	3.3	74.5		0.1	0.1		0.2	0.3	0.2	0.1		1.06	1055	1.050	1.053
Brain	10.7	14.5	2.2	71.2		0.4	0.2		0.2	0.3	0.3			1.04	1037	1.035	1.040
Breast	10.6	33.2	3.0	52.7		0.1	0.1		0.2	0.1				1.02	1003	1.014	1.029
Cell nucleus	10.6	9.0	3.2	74.2		2.6			0.4					1.00	1003	0.994	0.996
Eye lens	9.6	19.5	5.7	64.6		0.1	0.1		0.3	0.1				1.07	1050	1.055	1.060
GI tract	10.6	11.5	2.2	75.1		0.1	0.1		0.1	0.2	0.1			1.03	1023	1.024	1.028
Heart	10.3	12.1	3.2	73.4		0.1	0.1		0.2	0.3	0.2	0.1		1.06	1055	1.051	1.054
Kidney	10.3	13.2	3.0	72.4	0.1	0.2	0.2		0.2	0.2	0.2			1.05	1043	1.041	1.045
Liver	10.2	13.9	3.0	71.6		0.3	0.2		0.3	0.2	0.3			1.06	1053	1.050	1.054
Lung (deflated)	10.3	10.5	3.1	74.9		0.2	0.2		0.3	0.3	0.2			1.05	1044	1.041	1.044
Lung (inflated)														0.26	259	0.258	0.258
Lymph	10.8	4.1	1.1	83.2			0.3		0.1	0.4				1.03	1028	1.026	1.027
Muscle	10.2	14.3	3.4	71.0		0.2	0.1		0.3	0.1	0.4			1.05	1042	1.040	1.044
Ovary	10.5	9.3	2.4	76.8		0.2	0.2		0.2	0.2	0.2			1.05	1045	1.043	1.046
Pancreas	10.6	16.9	2.2	69.4		0.2	0.2		0.1	0.2	0.2			1.04	1032	1.034	1.041
Cartilage	9.6	9.9	2.2	74.4		2.2	0.5		0.9	0.3				1.10	1098	1.083	1.081
Red marrow	10.5	41.4	3.4	43.9		0.1			0.2	0.2	0.2	0.1		1.03	1014	1.023	1.041
Spongiosa	8.5	40.4	2.8	36.7	7.4	3.4	0.1	0.1	0.2	0.2	0.1	0.1		1.18	1260	1.150	1.156
Yellow marrow	11.5	64.4	0.7	23.1			0.1		0.1	0.1				0.98	958	0.982	1.013
Skin	10.0	20.4	4.2	64.5		0.1	0.2		0.2	0.3	0.1			1.09	1075	1.078	1.084
Spleen	10.3	11.3	3.2	74.1		0.3	0.1		0.2	0.2	0.3			1.06	1054	1.051	1.054
Testis	10.6	9.9	2.0	76.6		0.1	0.2		0.2	0.2	0.2			1.04	1032	1.032	1.035
Thyroid	10.4	11.9	2.4	74.5		0.1	0.2		0.1	0.2	0.1		0.1	1.05	1040	1.041	1.045
Skeleton—cortical bone	3.4	15.5	4.2	43.5	22.5	10.3	0.1	0.2	0.3					1.92	2376	1.781	1.714
Skeleton—cranium	5.0	21.2	4.0	43.5	17.6	8.1	0.1	0.2	0.3					1.61	1903	1.517	1.480
Skeleton—femur	7.0	34.5	2.8	36.8	12.9	5.5	0.1	0.1	0.2	0.1				1.33	1499	1.278	1.269
Skeleton—humerus	6.0	31.4	3.1	36.9	15.2	7.0	0.1	0.1	0.2					1.46	1683	1.389	1.370
Skeleton—mandible	4.6	19.9	4.1	43.5	18.7	8.6	0.1	0.2	0.3					1.68	2006	1.577	1.534
Skeleton—ribs (2nd, 6th)	6.4	26.3	3.9	43.6	13.1	6.0	0.1	0.1	0.3	0.1	0.1			1.41	1595	1.347	1.329
Skeleton—ribs (10th)	5.6	23.5	4.0	43.4	15.6	7.2	0.1	0.1	0.3	0.1	0.1			1.52	1763	1.441	1.413
Skeleton—sacrum	7.4	30.2	3.7	43.8	9.8	4.5		0.1	0.2	0.1	0.1	0.1		1.29	1413	1.244	1.238
Skeleton—spongiosa	8.5	40.4	2.8	36.7	7.4	3.4	0.1	0.1	0.2	0.2	0.1	0.1		1.18	1260	1.150	1.156
Skeleton—vertebral column (C4)	6.3	26.1	3.9	43.6	13.3	6.1	0.1	0.1	0.3	0.1	0.1	0.1		1.42	1609	1.355	1.337
Skeleton—vertebral column (D6, L3)	7.0	28.7	3.8	43.7	11.1	5.1		0.1	0.2	0.1	0.1	0.1		1.33	1477	1.278	1.267

4.2. Comparison of different calibrations with measurements

In the last section it was shown that the stoichiometric calibration based on the chemical composition of tissues is better defined than the usual tissue substitute calibration. In this section we show that the stoichiometric calibration is more precise in predicting relative proton stopping powers and relative electron densities. To this purpose we show the stoichiometric calibration (A) as the solid line in figure 2. For a comparison two tissue substitute calibrations were selected using either Mylar/Melinex/PTFE (B) or B110/SB5 (C) as a bone substitute. The CT data of the sheep's head were converted to relative proton stopping power according to the three different calibrations. The three resulting integrated proton stopping power matrices were compared to the measured one by computing the histogram of the difference between measurement and calculation for each matrix element. Figure 4 shows these curves for the three calibrations A, B and C represented by the solid, dotted and dashed line, respectively. The standard deviation, the mean deviation, the maximum absolute deviation and the number of matrix elements corresponding to deviations larger than 2% and 3% are listed together in table 5.

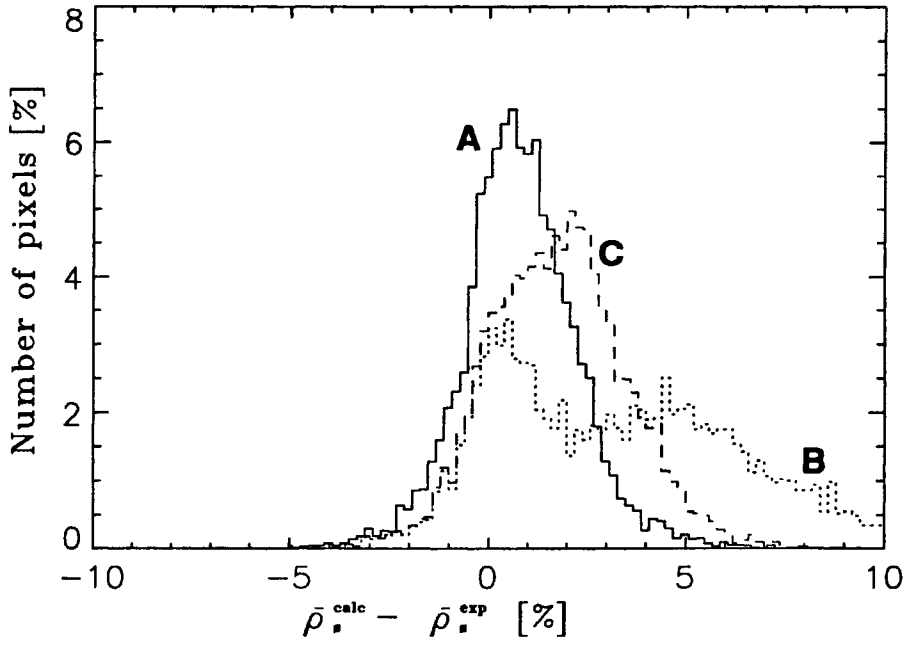

Figure 4. A histogram of differences between computed and measured integrated proton stopping power. The plot shows the number of pixels as a function of their deviation: the solid line for the stoichiometric calibration (A), the dotted line for the tissue substitute calibration with Mylar/Melinex/PTFE (B) and the dashed line for the tissue substitute calibration with B110/SB5 (C).

This comparison indicates that the stoichiometric calibration (A) is more appropriate to calibrate CT images.

Table 5. Differences between measurement and simulation with a particular calibration. In the table the maximum, the mean and the standard deviation are listed as percentages. The number of pixels N_p exceeding 2% and 3% difference between measurement and calculation is also given as a percentage.

Calibration	Maximum absolute deviation (%)	Mean deviation (%)	RMS deviation (%)	N_p for 2% deviation	N_p for 3% deviation
A. Stoichiometric	8.9	0.5	1.4	14.7	4.7
B. Tissue substitute: Mylar/Melinex	19.2	2.5	4.2	43.8	37.2
C. Tissue substitute: B110/SB5	10.3	1.2	2.1	32.4	16.0

5. Discussion

Several points emerge from the results summarized in the last section. The first point is that tissues can be well characterized by a fit to the ICRP tissue data as we give above (calibration A). The experimental data are in good agreement with this fit.

Secondly, tissue substitute calibrations should be used with caution. They do not necessarily lie on a unique curve, nor do they lie on average on the same curve as the ICRP tissues as can be seen in figures 2 and 3.

We think the problem of calibrating CT data directly with tissue substitutes has its origin in the chemical composition of the substitutes. It is not possible to produce tissue substitutes with exactly the same composition and density as real tissues. Small changes in e.g. the hydrogen content can produce significant differences in the proton stopping power. Additionally the tissue substitutes are usually produced for applications in radiation dosimetry and radiobiology (ICRU 1989) and do not necessarily fulfill the requirements for radiotherapy.

As we have shown, relative electron density and relative proton stopping power are closely related for tissues, so our experimental results with protons support the use of the stoichiometric calibration also for x-ray radiotherapy.

Our recipe for anyone who wants to develop a stoichiometric calibration curve is as follows.

(i) Choose some tissue substitutes with known chemical composition and physical density. It should be noted that these tissue substitutes do not necessarily have to be very tissue-like. It is possible to choose e.g. Lucite, Teflon, Delrin etc.

(ii) Scan the tissue substitutes in the CT scanner which is used for radiotherapy treatment planning and obtain the corresponding Hounsfield values.

(iii) Parametrize by using the information of chemical composition and measured Hounsfield values the CT unit. Fit this information to equations (5) and (8) and obtain the coefficients K^{ph}, K^{coh} and K^{KN}.

(iv) Compute the Hounsfield values of selected ICRP tissues of table 4 by putting them into equations (5) and (8) and compute the corresponding Hounsfield value.

(v) Calculate with the knowledge of the chemical composition of the selected ICRU tissues with formula (1) the relative electron density (x-ray radiotherapy) or with formula (3) the relative proton stopping power (proton therapy).

(vi) Make the appropriate fit through the data points to generate the final calibration curve.

Acknowledgment

The authors would like to express their appreciation to Professor Michael Goitein for careful reading of the manuscript.

References

Battista J J, Rider W D and van Dyke J 1980 Computed tomography for radiotherapy planning *Int. J. Radiat. Oncol. Biol. Phys.* **6** 99–107

Bichsel H 1972 Passage of charged particles through matter *American Institute of Physics Handbook* (New York: McGraw-Hill) pp 8-142–89

Chen G, Singh R, Castro J, Lyman J and Quivey J 1979 Treatment planning for heavy ion radiotherapy *Int. J. Radiat. Biol. Phys.* **5** 1809–19

Constantinou C 1974 Tissue substitutes for particulate radiations and their use in radiation dosimetry and radiotherapy *PhD Thesis* London University

Constantinou C and Harrington J 1992 An electron density calibration phantom for CT-based treatment planning computers *Med. Phys.* **19-2** 325–7

ICRP 1975 Report of the Task Group on Reference Man *ICRP Publication* 23

ICRU 1989 Tissue Substitutes in Radiation Dosimetry and Measurement *ICRU Report* 44

Jackson D F and Hawkes D J 1981 X-ray attenuation coefficients of elements and mixtures *Phys. Rep.* **70** 169–233

Janni J F 1982 Proton range-energy tables *At. Data Nucl. Data Tables* **27** 212–425

McCullough E C and Holmes T W 1985 Acceptance testing computerized radiation therapy treatment planning systems: direct utilization of CT scan data *Med. Phys.* **12** 237–42

Moyers M, Miller D, Siebers J, Galindo R, Sun S, Sardesai M and Chan L 1993 Water equivalence of various materials for 155 to 250 MeV protons, private communication

Mustafa A and Jackson D 1983 The relation between x-ray CT numbers and charged particle stopping powers and its significance for radiotherapy treatment planning *Phys. Med. Biol.* **28** 169–76

Rutherford R A, Pullan B R and Isherwood I 1976 Measurement of effective atomic number and electron density using an EMI scanner *Neuroradiology* **11** 15–21

Schneider U and Pedroni E 1995 Proton radiography as a tool for quality control in proton therapy *Med. Phys.* **22** 353–63

Woodard H C 1962 The elementary composition of human cortical bone *Health Phys.* **8** 513–7